

# High statistics measurements of pedestrian dynamics

July 27, 2021

ALESSANDRO CORBETTA

CASA- Centre for Analysis, Scientific computing and Applications,  
Department of Mathematics and Computer Science, Eindhoven University of Technology,  
P.O. Box 513, 5600 MB Eindhoven, The Netherlands,  
Department of Structural, Geotechnical and Building Engineering,  
Politecnico di Torino, Corso Duca degli Abruzzi 24, 10126 Torino, Italy

LUCA BRUNO

Department of Architecture and Design,  
Politecnico di Torino, Viale Mattioli 39, 10125, Torino, Italy

ADRIAN MUNTEAN

CASA- Centre for Analysis, Scientific computing and Applications,  
ICMS - Institute for Complex Molecular Systems  
Department of Mathematics and Computer Science, Eindhoven University of Technology,  
P.O. Box 513, 5600 MB Eindhoven, The Netherlands,

FEDERICO TOSCHI

Department of Physics and Department of Mathematics and Computer Science,  
Eindhoven University of Technology, P.O. Box 513, 5600 MB Eindhoven, The Netherlands,  
CNR-IAC, Via dei Taurini 19, 00185 Rome, Italy,

## Abstract

Understanding the complex behavior of pedestrians walking in crowds is a challenge for both science and technology. In particular, obtaining reliable models for crowd dynamics, capable of exhibiting qualitatively and quantitatively the observed emergent features of pedestrian flows, may have a remarkable impact for matters as security, comfort and structural serviceability. Aiming at a quantitative understanding of basic aspects of pedestrian dynamics, extensive and high-accuracy measurements of pedestrian trajectories have been performed. More than 100.000 real-life, time-resolved trajectories of people walking along a trafficked corridor in a building of the Eindhoven University of Technology, The Netherlands, have been recorded. A measurement strategy based on Microsoft Kinect<sup>TM</sup> has been used; the trajectories of pedestrians have been analyzed as ensemble data. The main result consists of a statistical descriptions of

pedestrian characteristic kinematic quantities such as positions and fundamental diagrams, possibly conditioned to local crowding status (e.g., one or more pedestrian(s) walking, presence of co-flows and counter-flows).

## 1 Introduction

Understanding the behavior of pedestrians walking in crowds is a complex challenge for both science and technology. Pedestrians have been proved to walk reflecting collective behaviors, which result from self-organized processes based on local interactions among individuals (cf. e.g. [6, 10, 13]). Obtaining reliable mathematical models for the dynamics of crowds, capable of exhibiting qualitatively and quantitatively these emergent features, may hence have a remarkable impact for matters as security ([12, 7]), comfort and structural serviceability ([11, 4]).

At the present time the largest part of crowd dynamics models are still missing a systematic experimental verification. This is probably due to a combination of several factors: firstly, the large variability in pedestrian crowds, flow conditions and geometries; secondly, the difficulty and partial inadequacy of measurement tools to resolve pedestrian motion, which often call for well controlled laboratory conditions to achieve higher reliability ([2, 8]). The quality and quantity of data are of course of paramount importance to validate crowd dynamics models beyond the most basic aspects such as e.g. mean velocity.

It is worth noticing that the use of laboratory conditions may fix constraints on both the possible geometries as well as on the actual “behavior” of the participants. Moreover, it may impose a physical limitation in the statistical exploration of human walking behavior because inter-subject and intra-subject variabilities ([20]) may be reduced or neglected.

Our goal is to be able to develop tools capable to enable the investigation of the dynamics of pedestrian crowds at extremely high-statistics and with high-quality recordings in real-life settings. It is common experience that complex systems can display statistics that strongly deviate from Gaussian normal distributions. This is for example the case of the dynamics of small particle matter in turbulent flows (see [17]). From that field of research we borrow both the techniques to accurately reconstruct pedestrian trajectories (by means of software developed for Particle Tracking Velocimetry, see [16]) as well as the statistical observables that allow to statistically quantify the phenomenology of crowds and thus make the quantitative comparison with model possible.

In this framework, we report on a few basic preliminary explorations of the crowd dynamics measurements we recently conducted. In Section 2, we describe our measurements set-up inspired by the work by [14] which allowed the *in-vivo* measurement of more than 100.000 pedestrians. Then we list a few features of the data ensemble built in Section 3. Finally, we close the paper with the discussions in Section 4.

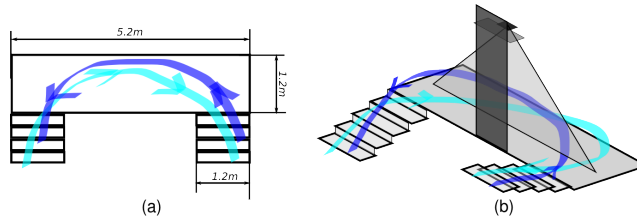


Figure 1: Schematics of the considered corridor. (a) top view; (b) three dimensional view. The bright arrow identifies the direction going from left to right ( $2R$ , ascending the stairs), the dark arrow otherwise ( $2L$ , descending the stairs).

## 2 The installation

A relatively highly trafficked corridor at Eindhoven University of Technology has been chosen as measurement site. The corridor connects the canteen of the “Metaforum” building to its dining area and it is crossed by approximately 2.200 pedestrians every day. The observed location serves as a landing between two different levels of the building, hence it is globally U-shaped and has staircases at its endings (see Fig. 1 for a geometric reference). The presence of the stairs induces a natural asymmetry between the two span-wise walking actions: in particular, pedestrians going to the right are *ascending* the stairs, whilst pedestrians going to the left are *descending*. Even in such a simple, although common, configuration many different walking scenarios might occur. In the simplest case, pedestrians walk alone, *undisturbed* in their motion by the presence of peers. On the other hand, when more than one person is present, either a *co-flow* or a *counter-flow* condition might happen. In the co-flow case, all pedestrians walk in the same direction, while, in counter-flow case, a bi-directional flow occurs. It is important to highlight that the data collected in this work do not refer to pedestrians instructed *a-priori* to cross the landing (as common in many “laboratory” crowd experiments); rather, they refer to the actual, unbiased, “field” measurement of pedestrian traffic.

The central, straight, section of the measurement site has been recorded via a Microsoft Kinect<sup>TM</sup> special camera (see [9]) on a 24/7 basis and with a temporal resolution of  $15Hz$ . The Kinect<sup>TM</sup> is able to provide, on side of the ordinary “color” picture of a target scene, that we disregarded, the depth map: namely the distance map between every recorded pixel and the camera plane (analogous to the one reconstructed in [2] by means of pairs of cameras). This allows the development of pedestrian detection algorithms with higher reliability.

The sensor has been located at an overhead altitude of  $4m$ , which allows a recording window of span-wise length  $3m$  (of which only  $2.2m$  have been kept for accuracy reasons) and of width  $1.2m$  (i.e., the entire chord).

The sequence of depth maps provided by the sensor is streamed to a processing unit which, as explained in the next Section, operates a pedestrian head

detection algorithm on a frame-by-frame basis and then a multi-particle (head) tracking.

## 2.1 Pedestrian detection and head tracking algorithms

The pedestrian detection algorithm is hereby concisely reported. For more extensive insights, the reader can refer to the appendix in [3] and to the original work by [14]. The latter reference contains also reliability estimates for the method.

Let  $f^n = f^n(\vec{z})$  be the depth map recorded by Kinect<sup>TM</sup> at time instant  $n \geq 0$  and at spatial position  $\vec{z} = (x, y)$ , i.e., in formulas,

$$f^n(\vec{z}) := \text{distance}(\text{element in } \vec{z}, \text{camera plane}). \quad (1)$$

To detect the positions of pedestrians in  $f^n$  the following steps are performed.

- 1. Depth-based significant foreground segmentation.** A common background  $B = B(\vec{z})$  (possibly built after suitable averages of “empty” recordings) is expected across different depth maps. The foreground  $\tilde{F}^n = \tilde{F}^n(\vec{z})$  is extracted via a thresholding operation

$$\tilde{F}^n(\vec{z}) \leftarrow f^n(\vec{z}) \cdot [f^n(\vec{z}) - B(\vec{z}) > \epsilon_1],$$

where  $\epsilon_1 > 0$  is a given (small) threshold, and  $[P(\vec{z})] = 1$  whenever proposition “ $P(\vec{z})$ ” holds true, and  $[P(\vec{z})] = +\infty$  otherwise.

Besides, the foreground is likely populated by elements which are not tall enough to be pedestrians, therefore a second thresholding operation is performed

$$F^n(\vec{z}) \leftarrow \tilde{F}^n(\vec{z}) \cdot [\tilde{F}^n(\vec{z}) > h].$$

Here,  $F^n = F^n(\vec{z})$  is the retained “significant” foreground and  $h$  denotes the typical distance among the waist of pedestrians and the camera plane.

- 2. Foreground random sampling.** The “dense” foreground depth map  $F^n$  is sampled and  $N$  of its points (having finite depth value) are randomly extracted. A “sparse” (cloud) representative of  $F^n$ ,

$$F_s^n = \{(\vec{z}_1, F^n(\vec{z}_1)), (\vec{z}_2, F^n(\vec{z}_2)), \dots, (\vec{z}_N, F^n(\vec{z}_N))\},$$

is hence built.

It is important to notice that the points left in  $F_s^n$  likely belong to the pedestrians in the scene and, if  $N$  is large enough ( $N = O(500)$ ), they provide a good approximation of the three dimensional geometry of the latter.

- 3. Foreground random cloud clusterization.** To identify and isolate pedestrians, sparse samples in  $F_s^n$  are agglomerated in clusters which are likely in 1 : 1 correspondence with pedestrians themselves.

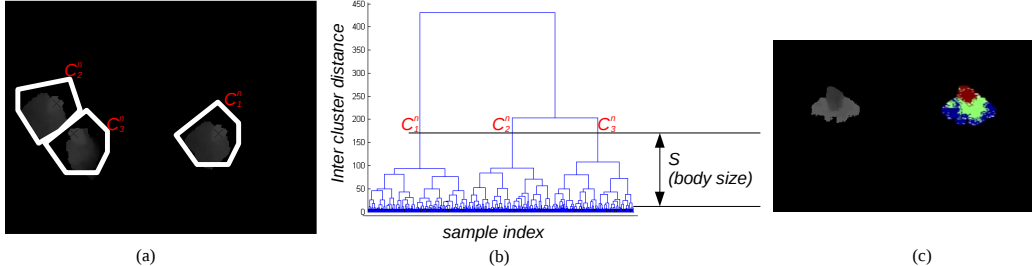


Figure 2: (a) Foreground of a depth map showing three pedestrians; (b) clusterization tree of the random sampled foreground. The tree is cut at height  $S$  and three different clusters, in correspondence with the pedestrians, are found; (c) (left) depth map of a single pedestrian as provided by Kinect; (right) random sampled version of the pedestrian. Colors identify region bounded by different depth percentiles: red (head), depth is less than the 10<sup>th</sup> percentile, green (shoulders), depth is between the 10<sup>th</sup> and the 50<sup>th</sup> percentile, blue (body), remaining points.

The agglomeration is performed via a *hierarchical clustering* operation based on the geometrical distance between points following a *maximum linkage* clustering (see, e.g., [5]).

Heuristically speaking, the sparse samples get iteratively agglomerated in a binary tree fashion forming larger and larger clusters. This iterative procedure merges clusters beginning from single points on the basis of their distance; closest pairs are merged first. Ideally, whenever a cluster  $C^n$  features a distance from all others clusters larger than the scale size  $S$  of the human body, then  $C^n$  corresponds to a single pedestrian.

From a formal point of view, the length  $S$  is adopted as cutoff parameter of the clusterization tree, and the clusters  $C_1^n, C_2^n, \dots, C_N^n$  underneath  $S$  correspond to pedestrians (see pedestrians in Fig. 2(a) which are identified via the clusterization tree in Fig. 2(b)).

4. **Head identification.** Each point in a given cluster  $C_i^n$  comes with a depth information; therefore, the probability distribution function of the depths in  $C_i^n$  can be considered. The largest part of probability mass is expected to be in the shoulder region, whilst the head marks a small probability area having least distance from the camera. As a consequence, the pedestrian head is identified as the set of points  $H_i^n \subset C_i^n$  such that they are closer to the camera than the 10<sup>th</sup> percentile of points in  $C_i^n$  (see Fig. 2(c)).
5. **Pedestrians tracking.** Pedestrians are tracked following the centroid of their heads,  $\vec{Z}_i^n = \text{mean}(H_i^n)$ , as they were particles. A tracking approach

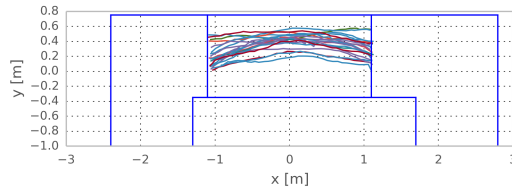


Figure 3: Twenty trajectories chosen randomly among the ones recorded throughout the experimental campaign. These trajectories have been followed by pedestrians walking undisturbed from right to left (2L).

analogous to Particle Tracking Velocimetry (PTV) from experimental fluid mechanics is chosen (for a general reference on the method, see e.g. [19]. The actual tracking of particles has been done via the OpenPTV library, see [16]). In Figure 3, we illustrate a random selection of final trajectories obtained via this method.

## 2.2 Ensemble data for pedestrian dynamics

Once pedestrian trajectories have been reconstructed, they are considered as elements of an ensemble (see [3]). In other words, every pedestrian is “confused” in terms of its trajectory with all the others. The analysis of such an ensemble allows one to isolate average behaviors as well as “unusual” ones. This analysis can be enriched by looking at specific flow conditions (e.g. single pedestrians, counter-flows, co-flows) at a time. In this work, we focus on the average behaviors intended as conditioned ensemble means. A study of the “unusual” behaviors will be considered in a future work.

## 3 Results

In this Section, we analyze the trajectories gathered from a measurement campaign lasted 50 working days, and which led to the tracking of more than 100.000 people. The trajectories spanned over more than 2.5 million depth frames in which up to 6 people were present at the same time (see Fig. 5(a)). In the following Subsections different kinds of analyses grounded on ensemble-means and depending on the local flow conditions are performed. Specifically in 3.1 a quantitative overview on the data is given; in 3.2 fundamental diagrams obtained from ensemble averages conditioned to the local pedestrian flow are considered; finally, in 3.3, heat maps elaborated from measured pedestrian positions are commented.

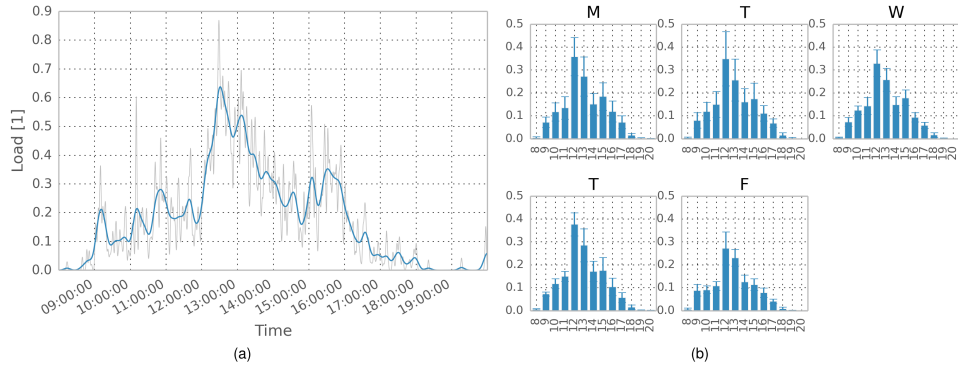


Figure 4: (a) Time averaged facility load during the 19<sup>th</sup> of June 2013, from 8AM to 8PM (width of the averaging windows: 1min - thin line, 5min - thick line); (b) facility load vs. the hour of the day during the weekdays in terms of mean value (bars) and standard deviation (error bars).

### 3.1 Pedestrian data features

The considered facility features different usage trends depending upon the moment of the day. We consider the load, defined as the number of pedestrians in the facility in a given instant of time, as primary usage indicator. In formulas it reads as

$$load(t) := \#\text{Pedestrians in the facility at time } t.$$

In particular, we use time-averaged values of the load to easily quantify the usage scenario as well as the most trafficked instants of the day. In Fig. 4(a), we show a day-long time history of the load. It shows two peaks: one at around 12PM (lunchtime in Eindhoven) and another one at around 3PM (break). This usage trend is homogeneous throughout the different weekdays as we report in Fig. 4(b), where hourly averaged load statistics depending on the day of the week are shown. From Fig. 4(b) one may notice that the usage is homogeneous across the weekdays with the exception of Fridays, in which the traffic is generally reduced by approximately 20%.

In Figure 5(a), we report the load distribution in dependence on the local flow condition. The scenario of one pedestrian walking undisturbed is the most common, and, in this case, the ascending direction (left to right) is the most frequent one. Up to five pedestrians have been observed in co-flow conditions in either directions and with comparable frequencies. Counter-flows appear to be more frequent whenever more than three pedestrians occupy the facility; this is not surprisingly as according to the definition given counter-flow cases include different combinations of the directions for any load greater than two. Up to six pedestrians have been observed in the counter-flow case.

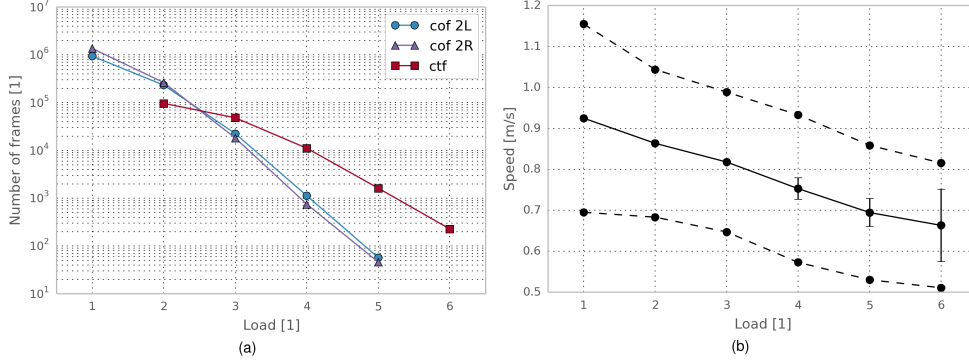


Figure 5: (a) Absolute frequency of load (amount of people in the facility) depending on the flow condition (co-flow of all pedestrians to the left (cof 2L) or to the right (cof 2R) or in presence of counter-flowing directions (ctf)). (b) Fundamental diagram: the ensemble-averaged frame-wise mean pedestrian speed is plotted in dependence on the local facility load, i.e., the amount of people in the facility (solid line). The standard deviation of the average frame-wise speed is reported in added and subtracted to the mean (dotted lines). Confidence on the ensemble mean values decreases as the load increases as high load are less likely to happen; the error bars portray the standard deviation of the ensemble means evaluated after splitting the data-set in four even sub-samples.

### 3.2 Fundamental diagrams

In this Subsection we consider a generalized version of the fundamental diagram in which the facility load is considered as a dependent variable (in place of the conventional pedestrian density, by virtue of the reduced area recorded) and it is compared with the pedestrian velocity (see, e.g., [15], [1] and [18] as a reference for conventional fundamental diagrams). Specifically, we consider the ensemble-mean, frame-wise averaged, pedestrian speed  $\bar{U}$  with respect to the instantaneous facility load and, possibly, flow conditions. In formulas,  $\bar{U}$  reads as

$$\bar{U}(\text{load} = L \mid \text{flow condition} = Q) := \text{mean}(\{ U^n, \text{ for all } n \text{ such that load} = L \text{ and flow condition} = Q \}),$$

where

$$U^n := \text{mean}(\{ \text{speed of pedestrians in } f^n \}),$$

and  $Q$  can be, e.g., the single pedestrian case, the co-flow case, the counter-flow case and so on.

In other words, all the time instants (frames) featuring a given load and flow conditions are grouped, then, the average frame-wise walking speed,  $U^n$ , is evaluated as an indicator of the “effective” walking speed in the frame. Finally,



to have an ensemble indicator, we extract ensemble means of such effective walking speeds  $\bar{U}$ .

In Figure 5(b), a fundamental diagram including all possible flow conditions is reported. The diagram, consistently with other experimental fundamental diagrams (see, e.g., [15]), shows a decreasing trend as the load increases; moreover it exhibits an approximately linear behavior. Pedestrians average speed drops from approximately  $0.92m/s$  - in the undisturbed case - to approximately  $0.68m/s$  - in the most loaded condition observed. An ensemble standard deviation on the  $\{U^n\}$  decreasing from  $0.23m/s$  to  $0.15m/s$  can be observed as the load increases. This fluctuation in the data is likely an effect the inter-subject and intra-subject variabilities (see, e.g., [20]).

Qualitative and quantitative changes in the fundamental diagram emerge when a restriction to the local flow  $Q$  is applied. Firstly, it is worth noting that fundamental diagrams in co-flow conditions (i.e., which consider, exclusively, pedestrians going to the left (2L) or going to the right (2R)) differ one another - see Fig. 6(a)). This reflects a “broken symmetry” relative to the walking direction. As a matter of facts, pedestrians moving toward the left side walk faster on average. This can be explained by considering that the facility is indeed a landing between two stair cases; pedestrians going to the left have just descended a ramp of stairs and for this reason they may be walking slightly faster. On the other hand, pedestrians going to the right have just climbed a ramp of stairs and for this reason they may be walking with a lower speed.

When the counter-flow condition is considered, we observe an effective speed which, for low values of the load, lies in between the two co-flow cases. This may also be the case at larger loads if one considers the larger statistics errors present for cases with more than four pedestrians.

Remarkably if we isolate pedestrians on the basis of their direction also in counter-flow conditions, we can see that velocities in the counter-flow cases are always higher or equal than the co-flow cases with the same load (see Fig. 6(b)). This suggests that the presence of counter-flows triggers a sort of self-organization which increases the overall performances in terms of effective speed. Similar effects have been observed also in [8], where pedestrian fluxes in counter-flows have been measured to be higher than the fluxes in analogous co-flow conditions.

### 3.3 Heat maps

In this Subsection, we analyze how pedestrians (head) positions  $\vec{Z} = (X, Y)$  distribute in probability as functions of the local flow conditions. Focus is given on the undisturbed pedestrian case and on two pedestrian counter-flow case.

Probability distribution functions of positions are reported as heat maps, which, *de facto*, express which portions of the floor are loaded with higher frequency. Clearly, as the facility is globally U-shaped, heat maps show a curved trend. This likely reflects an inertial-like behavior in the act of walking. Moreover, the very shape of the heat maps appears to be depending both by the walking direction as well as altered by the local traffic conditions.

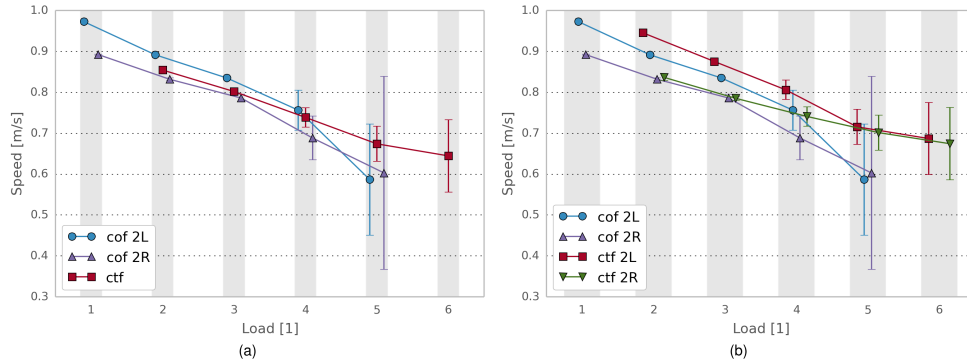


Figure 6: Fundamental diagrams conditioned to the local flow. The ensemble-averaged frame-wise mean pedestrian speed is plotted in dependence of the local load, in co-flow (all pedestrians have the same direction, cof) condition and in counter-flow condition (at least two pedestrians have different directions, ctf). Both cases of pedestrians going to the left (2L) and to the right (2R) are considered. (a) Counter-flow cases are considered independently on the direction; (b) counter-flow cases are considered dependently on the direction. Fundamental diagrams have been slightly shifted on the load axis (which can assume only integer values) for enhanced readability. Confidence on the ensemble mean values decreases as the load increases as high load are less likely to happen; the error bars portray the standard deviation of the ensemble means evaluated after splitting the data-set in four even sub-samples. As the condition of co-flow with  $load = 5$  is very unlikely to happen just few measurements have been collected, hence the large statistical error.

In Figure 7, the heat maps referring to pedestrians walking undisturbed either from the left to the right side of the facility (Fig. 7(a)) or vice-versa (Fig. 7(b)), are reported. Pedestrian positions heavily concentrate in a thin layer (say  $l = l(x)$ ) of approximate width of *ca.* 20cm.

To compare heat maps with greater ease, a *reduced* version of the latter containing just the layer boundaries is considered. Specifically, for each chord-wise section of the facility  $x$ , local means and local standard deviations of positions, i.e.  $mean(Y|X = x)$  and  $std(Y|X = x)$ , are evaluated. Hence, for each section,  $l = l(x)$  is approximated as

$$l(x) \approx \{y : |y - mean(Y|X = x)| \leq std(Y|X = x)\}.$$

In Figure 8(a), reduced heat maps for single, undisturbed, pedestrians are reported. Pedestrians, even if free to occupy every region of the corridor, appear to “naturally” walk slightly closer to the wall placed at the right hand side of the walker. No other qualitative difference in the thin layer geometry is observed - see Fig. 8(b) for a qualitative comparison.

This natural tendency of keeping the right gets heavily emphasized in pres-

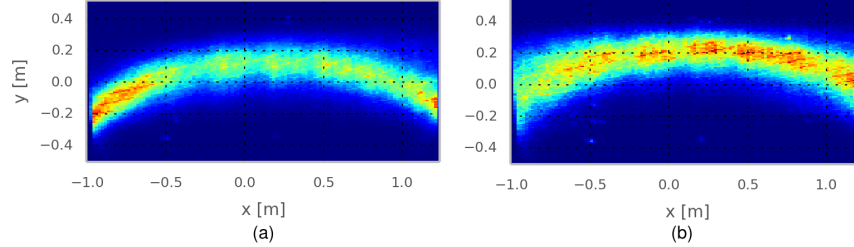


Figure 7: Heat maps, i.e. probability distribution functions, of pedestrians head position. The maps consider undisturbed pedestrians going to the left (a) and to the right (b). Low probability positions are in blue, high probability positions are in red.

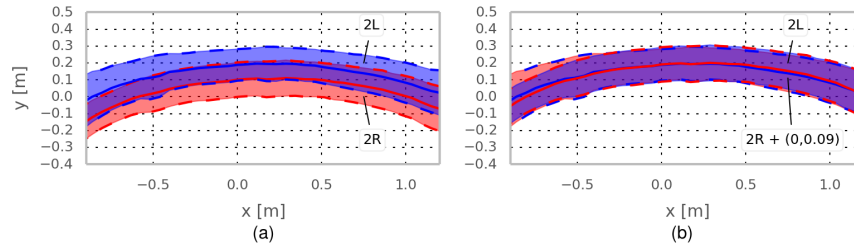


Figure 8: (a) Reduced heat maps referring to undisturbed pedestrians going left (2L, blue) and right (2R, red); (b) heat maps from (a) are superimposed by a vertical shift in upward direction of the 2R map (red,  $\Delta y = .09m$ ). The maps feature no qualitative difference than the vertical (chord-wise) translation.

ence of a second pedestrians having opposite direction with respect to the observed one, i.e., in the simplest counter-flow condition. In Figure 9(a) and (b), the heat maps of undisturbed pedestrians are compared with the analogous ones in counter-flow conditions. Pedestrians positions appear to be pushed to the (relative) right hand sides in close contact with the wall. In this condition a sort of “spontaneous organization” seems to emerge. This observation is in agreement with laboratory measurements (cf. e.g. with [8], in which complex counter-flows have been experimentally induced and analyzed, and with [10], in which the bias pedestrians have in choosing mutual avoidance direction has been inquired).

## 4 Discussion

In this work a large number of pedestrian trajectories has been collected and analyzed as ensemble data. The data collection procedure is grounded on the recording of overhead depth maps - obtained by means of Microsoft Kinect<sup>TM</sup>-

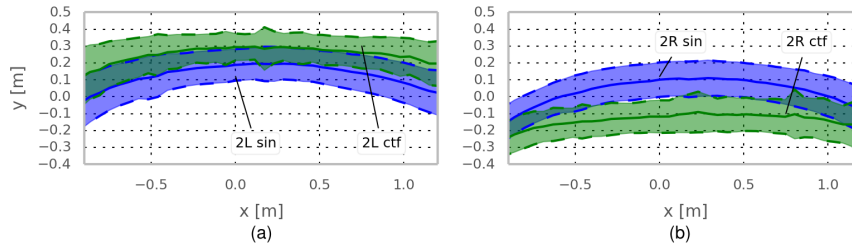


Figure 9: Heat maps conditioned to the flow. Synthetic heat maps of pedestrians going left (a) and right (b) are compared for the undisturbed case (sin, blue) and the two pedestrians counter-flow case (ctf, green). The vertical shift is determined by the flow condition.

which allowed the detection of pedestrian heads. Head tracking was carried out by Particle Tracking Velocimetry based techniques.

The data, taken during an experimental campaign lasted fifty working days, refers to all pedestrians walking on a landing in Eindhoven University of Technology. Recorded pedestrians are expected not to be biased by the recording campaign as no factual modification of the facility is observable in the ordinary use.

The obtained trajectories spread among different flow conditions, from the single undisturbed pedestrian case, to the co-flow or the counter flow cases which involve many pedestrians. Respectively, in the co-flow case every pedestrian walks in the same direction, while, in the counter-flow cases, at least two opposite directions are observed.

We presented here preliminary results, while our experiment is collecting additional statistics that will be particularly important to improve the quality of statistics at higher loads. Trajectories mostly concentrate at lunch hours, in which the facility load shows to be homogeneous across the weekdays with the exception of Fridays in which a 20% reduction of the traffic is noticeable. Most frequently, just one pedestrian is present in the facility; nonetheless, up to five pedestrians have been recorded while walking in co-flow and up to six in counter-flow. As a consequence, very rich statistics have been collected for loads smaller or equal than four, but yet not enough for loads corresponding to five or larger number of pedestrians.

Data has been treated in a statistical fashion including various kind of averages, possibly conditioned to the flow. Specifically, ensemble means of average pedestrians frame-wise speed have been considered. These allowed us to obtain fundamental diagrams comparing speeds vs. the local loads. Our fundamental diagrams show that co-flow speed are higher for descending pedestrians than for ascending ones (at least up to load four, where statistically significant estimates of speeds have been obtained). Moreover, speeds in counter-flows appear to be higher than in corresponding co-flows. This fact may be related to some kind of spontaneous organization. This organization may be also noticed in heat maps

- i.e., ensemble averages of spatial positions. A shifting on the average position of pedestrians toward the right side of the corridor has been measured when counter-flows occur. The obtained results are likely to feature a dependence on the specific geometry considered; further experiments on more generic geometric settings are ongoing.

## Acknowledgments

We would like to thank A. Holten and G. Oerlemans for the help with the installation of the Kinect<sup>TM</sup> sensor in the MetaForum building at the Eindhoven University of Technology. We thank A. Liberzon (Tel Aviv, Israel) for his precious help with the adaption of the Particle Tracking software to our project and A. Tosin (CNR-IAC Rome, Italy) for the useful discussions. We acknowledge the Brilliant Streets research program of the Intelligent Lighting Institute at the Eindhoven University of Technology. AC was founded by a Lagrange Ph.D. scholarship granted by the CRT Foundation, Turin, Italy and by the the Eindhoven University of Technology, The Netherlands.

## References

- [1] Nicola Bellomo and Christian Dogbe. On the modeling of traffic and crowds: A survey of models, speculations, and perspectives. *SIAM review*, 53(3):409–463, 2011.
- [2] Maik Boltes and Armin Seyfried. Collecting pedestrian trajectories. *Neurocomputing*, 100:127–133, 2013.
- [3] Alessandro Corbetta, Adrian Muntean, Federico Toschi, and Kiamars Vafayi. Parameter estimation of social forces in crowd dynamics models via a probabilistic method. (*submitted*), 2014.
- [4] Pat Dallard, Tony Fitzpatrick, Anthony Flint, Angus Low, Roger Riddill Smith, Michael Willford, and Mark Roche. London millennium bridge: pedestrian-induced lateral vibration. *Journal of Bridge Engineering*, 6(6):412–417, 2001.
- [5] Richard O Duda, Peter E Hart, and David G Stork. *Pattern Classification*. John Wiley & Sons, 2012.
- [6] Dirk Helbing and Anders Johansson. *Pedestrian, crowd and evacuation dynamics*. Springer, 2009.
- [7] Dirk Helbing and Pratik Mukerji. Crowd disasters as systemic failures: analysis of the love parade disaster. *EPJ Data Science*, 1(1):1–40, 2012.
- [8] Tobias Kretz, Anna Grnebohm, Maike Kaufman, Florian Mazur, and Michael Schreckenberg. Experimental study of pedestrian counterflow in

- a corridor. *Journal of Statistical Mechanics: Theory and Experiment*, 2006(10):10001, 2006.
- [9] Microsoft Corp. Kinect for Xbox 360, available online: <http://www.xbox.com/en-us/kinect/>, 2011. Redmond, WA, USA.
- [10] Mehdi Moussaïd, Dirk Helbing, Simon Garnier, Anders Johansson, Maud Combe, and Guy Theraulaz. Experimental study of the behavioural mechanisms underlying self-organization in human crowds. *Proceedings of the Royal Society B: Biological Sciences*, pages rspb-2009, 2009.
- [11] Shun-ichi Nakamura and Toshitsugu Kawasaki. Lateral vibration of foot-bridges by synchronous walking. *Journal of Constructional steel research*, 62(11):1148–1160, 2006.
- [12] Andreas Schadschneider, Wolfram Klingsch, Hubert Klüpfel, Tobias Kretz, Christian Rogsch, and Armin Seyfried. Evacuation dynamics: Empirical results, modeling and applications. In *Encyclopedia of complexity and systems science*, pages 3142–3176. Springer, 2009.
- [13] Andreas Schadschneider and Armin Seyfried. Empirical results for pedestrian dynamics and their implications for cellular automata models. *Pedestrian Behavior: Data Collection and Applications*, pages 27–43, 2009.
- [14] Stefan Seer, Norbert Brändle, and Carlo Ratti. Kinects and human kinetics: a new approach for studying crowd behavior. (*submitted*), 2012.
- [15] Armin Seyfried and Andreas Schadschneider. Fundamental diagram and validation of crowd models. In *Cellular Automata*, pages 563–566. Springer, 2008.
- [16] The OpenPTV Consortium. OpenPTV: Open source particle tracking velocimetry, 2012–.
- [17] Federico Toschi and Eberhard Bodenschatz. Lagrangian properties of particles in turbulence. *Annual Review of Fluid Mechanics*, 41:375–404, 2009.
- [18] Fiammetta Venuti and Luca Bruno. An interpretative model of the pedestrian fundamental relation. *Comptes Rendus Mécanique*, 335(4):194–200, 2007.
- [19] Jochen Willneff. A Spatio-Temporal Matching Algorithm for 3D Particle Tracking Velocimetry. *Mitteilungen-Institut für Geodäsie und Photogrammetrie an der Eidgenössischen Technischen Hochschule Zürich*, 2003.
- [20] Stana Živanović, Aleksandar Pavić, and Paul Reynolds. Probability-based prediction of multi-mode vibration response to walking excitation. *Engineering Structures*, 29(6):942–954, 2007.